Available online at www.sciencedirect.com

ScienceDirect

Solar Energy 111 (2015) 264–276

SOLAR ENERGY

www.elsevier.com/locate/solener

Least square based method for the estimation of the optical end loss of linear Fresnel concentrators

Marcos Hongn, Silvana Flores Larsen *, Marcelo Gea, Martín Altamirano

Instituto de Investigaciones en Energía No Convencional (INENCO), Universidad Nacional de Salta – CONICET, Avenida Bolivia 5150, CP 4400 Salta Capital, Argentina

Received 12 June 2014; received in revised form 27 October 2014; accepted 30 October 2014

Communicated by: Associate Editor Robert Pitz-Paal

Abstract

Small-scale solar concentrators based on Linear Fresnel Collectors (LFC) are a promising technology for domestic and industry applications. In such small systems, optical end losses and their influence on the energy performance are crucial issues. Although ray tracing is the most used method to estimate end losses, a less detailed and less time-consuming procedure is the analytical method, based on the equations that describe the sun and mirror positions. This method was used in this paper to study the behavior of the optical end losses with latitude and LFC geometry. A simple least square fitting expression was proposed to estimate the average annual non-illuminated length and the end loss factor for any latitude – between 0° and ±40° – and for any LFC azimuth. In particular, instantaneous, daily and annual periods at different latitudes for a North–South tracking LFC were analyzed. Finally, the instantaneous non-illuminated length on a short LFC system in Salta city, Argentina (24.7°S, 65.4°W) was experimentally determined through digital imaging analysis. A good agreement between the theoretical and the experimental values was found with average RMSE values of 6%.

Keywords: Annual end loss estimation; Small-scale linear Fresnel concentrator; Non-illuminated length

1. Introduction

Concentrating solar collectors have grown in popularity in the last decades because they provide a promising and non-polluting method to transform the solar energy into electricity or thermal power. Among concentrating collectors, Linear Fresnel Collectors (LFC) have become a profitable technology for large scale solar energy collection, so there is extensive literature covering a wide variety of topics related to long absorbers. Contrary to large LFC systems, some applications do not require such long receivers, which offer a great opportunity to develop small LFC equipments. In fact, historically, most LFC were developed for low or medium-temperature heat generation (Zhu, 2013). For example, small-scale systems with heat output in the range of 150–300 °C are suitable to be used in the heating/cooling of buildings (Bermejo et al., 2010), domestic water heating (Sultana et al., 2012), steam generation for mining, in textile and chemical industries, and also in agricultural, timber and food applications (Häberle et al., 2006; Rawlins and Ashcroft, 2013). The large variety of possible applications of small systems is promissory, but further research is needed in order to characterize their optical performance along the year. One of the factors affecting the whole optical performance of LFCs is the end loss produced by the portion of the absorber that is not illuminated by the mirror field and it has direct influence on the optical

* Corresponding author. Tel.: +54 387 4255578.
E-mail address: seflores@unsa.edu.ar (S.F. Larsen).

http://dx.doi.org/10.1016/j.solener.2014.10.042
0038-092X/

Nomenclature

A_{net}	net area of mirrors (m^2)
D_i	horizontal distance between the i mirror centerline and the solar absorber line projected on the aperture plane, positive when the mirror is at the west of the receiver (m)
D_{eff}	effective horizontal distance for reflector field characterization (m)
$f_{end,i}$	fraction of the absorber length that is reached by the sun rays reflected by the mirror i
$f_{end,i}^{daily}$	daily average of $f_{end,i}$ (unitless)
$f_{end,i}^{annual}$	annual average of $f_{end,i}$ (unitless)
F_i	focal distance of the i-mirror, the distance between the i-mirror centerline and the solar absorber (m)
F_{eff}	effective focal distance for reflector field characterization (m)
G_b	direct normal beam irradiance (W/m^2)
g_{corr}	corrective function, $0 \leqslant g_{corr} \leqslant 1$ (unitless)
H	height from the aperture plane to the absorber (m)
IAM	incidence angle modifier (unitless)
L_i	instantaneous non-illuminated length caused by the i mirror (m)
$\hat{L}_i$	adimensional non-illuminated length, $\hat{L}_i = L_i/H$ (unitless)
$\hat{L}_{daily,i}$	daily average $\hat{L}_i$ (unitless)
$\hat{L}_{annual,i}$	annual average $\hat{L}_i$ (unitless)
P_i	unit vector normal to the mirror surface, defined in Cartesian coordinates by $P_i = (x_i, y_i, z_i)$
P_s	unit vector describing the sun direction, in Cartesian coordinates $P_s = (x_s, y_s, z_s)$
Q_{abs}	solar irradiance that is absorbed by the receiver (W)
W_{field}	distance from the center of the field to the last mirror axis (m)
Z	absorber length (m)

Greek symbols

α_p	profile angle. It is the solar altitude angle projected on an east–west plane, $0 < \alpha_p < 180°$. Thus, $\alpha_p < 90°$ when $\gamma_s < 0°$
β_i	mirror slope, the angle between the plane of the surface and the horizontal, $0° \leqslant \beta_i \leqslant 90°$
γ	LFC azimuth angle, the deviation of the projection on a horizontal plane of the normal to the surface from the local meridian, with zero due south, east negative
γ_i	mirror azimuth angle, the deviation of the projection on a horizontal plane of the normal to the surface from the local meridian, with zero due south, east negative. For a North–South tracking mirror, $\gamma_i = \pm 90°$
γ_s	solar azimuth angle, the angular displacement from south of the projection of beam radiation on the horizontal plane, with zero due south, east negative (°)
δ	declination, the angular position of the sun at solar noon with respect to the plane of the Equator, north positive; $-23.45 \leqslant \delta \leqslant 23.45$ (°)
$\eta_{opt,0}$	optical efficiency at normal incidence (unitless)
θ_z	zenith angle, the angle between the vertical and the line to the sun (°)
ϕ	site latitude, negative to south (°)
ω	hour angle, the angular displacement of the sun east or west of the local meridian due to rotation of the earth on its axis at 15° per hour; morning negative, afternoon positive (°)

efficiency of the system. Due to the sun path in the sky, the non-illuminated length depends on the site latitude, the mirror field geometry and the orientation of the collector as well as on the month, day and hour when it is evaluated. At high latitudes, this length covers an important portion of the absorber, which significantly reduces its overall efficiency. On the other hand, North–South tracking orientation has been proved to have better performance than East–West tracking, but in the case of small concentrating collectors the shape and orientation of the land or roof does not allow an ideal N–S orientation, so the analysis of end losses should cover a range of possible orientations.

Ray-tracing is the usual method to estimate end losses. As it is a very detailed and time-consuming procedure, alternative mathematical equations were developed by different authors in the last years. Buie et al. (2002) analyzed the end effect of a North–South LFC and gave an approximate equation which estimates this effect at solar noon. Shaoxuan and Chaofeng (2011) derived the equation to estimate the instantaneous non-illuminated length for North–South and East–West LFC and they confirmed that this length increases with mirror focal distances for a North–South collector field at 25°01′N. For this latitude and configuration, the instantaneous non-illuminated length at solar noon on monthly average days was plotted as a function of the focal distance and the results were verified by ray-tracing simulation.

Instead of calculating the non-illuminated length, Heimsath et al. (2014) recently proposed the use of a corrective end loss factor f_{end}, defined as the illuminated fraction of the absorber length. This factor, which accounts for the finite receiver length, is applied to the calculation of the collector performance:

$$\frac{\dot{Q}_{abs}}{A_{net} G_b} = \eta_{opt,0} IAM(\theta_z, \gamma_s) f_{end} \quad (1)$$

where $\dot{Q}_{abs}$ is the solar irradiance that is absorbed by the receiver (W), A_{net} is the net area of mirrors, G_b is the direct beam radiation (W/m^2), $\eta_{opt,0}$ the optical efficiency at normal incidence, and IAM the incidence angle modifier. IAM accounts for the cosine effect and for all optical loss factors that depend on the incidence angle and that diminish the optical efficiency, under the assumption of an infinite receiver. Heimsath et al. (2014) proposed to calculate the instantaneous end loss of an LFC using an effective height rather than the nominal height of the receiver. Using this effective height a better representation is obtained of the mean optical path length of the whole mirror field. They compared the computed instantaneous end loss factor to exact ray tracing simulations and they verified that for annual calculations the difference is rather small (below 0.5% for Abdali – latitude 30°, longitude 47.6° – and for a collector with 25 m length).

As shown, the equations for estimating end losses are currently well known and they can be used for yield simulations for any latitude, longitude or collector orientation. But a general simple expression to estimate the average annual non-illuminated length and end loss factor for any latitude has not been developed yet. Moreover, experimental measurements of the optical end loss are not available in the literature. The aim of this paper is to develop simple expressions to estimate the average annual non-illuminated length and the end loss factor at any latitude and azimuth of a rectangular LFC. As explained before, because small scale collectors are often installed according to the available land/roof with slight deviation to North–South, in this paper a general expression for any orientation was obtained, and a deeper analysis for North–South orientation was performed. The instantaneous, daily and annual adimensional non-illuminated length were defined and studied for different latitudes and mirror–receiver distances. Simplified expressions that estimate the annual non-illuminated length and the annual end loss factor for any latitude and LFC azimuth were obtained through a least square fitting method. Finally, experimental measurements on a short LFC system in Salta city (24.7°S, 65.4°W) were performed and theoretical and experimental results were compared and discussed.

2. Method

This section explains the method used to estimate the instantaneous and average end loss factor of a short North–South LFC, as a function of the receiver length and height, the mirror distance and the site latitude. The studied LFC consists of N nearly flat mirrors that track the sun during daytime and a central fixed receiver. This receiver of length Z is placed at a height H from the aperture plane, as shown in Fig. 1. D_i is the horizontal distance between the i mirror centerline and the absorber (D_i is positive when the mirror is at the west side of the receiver).

L_i is the instantaneous non-illuminated length caused by the i mirror and it can be estimated from geometrical considerations (Appendix A). Because mirrors are placed at different distances from the absorber, it is evident that each mirror produces a different L_i on the receiver at the same time. The following simplifying assumptions were made in order to calculate L_i:

- The solar rays are parallel, that is, the effect of sun shape is not considered. Sun position was calculated through Spencer's relationship given in Duffie and Beckman (2006).
- The mirror is an ideal specular surface; mirror errors are not considered.
- The mirror and the receiver have the same length and the same alignment.
- The reflection is calculated in the central axis of the mirror.

These simplifications are ideal pictures of the reality. In fact, in real mirrors, the slope of the surface at many points of the mirror is different from the ideal mirror which is the main sources of the optical errors (Ulmer et al., 2009). Huang and Han (2012) found that the double of the slope error is a good approximation of the reflected ray error linear Fresnel reflectors. Zhu (2013) developed First OPTIC, an analytical approach that treats mirror slope error, as well as receiver position error, and collector tracking error as geometric modifications to the collector. Common accepted values are: mirror slope error of around 2 mrad, mirror tracking error of around 1 mrad, and receiver position error of around 0.035 m. A value of 0.8 mrad is commonly accepted to describe the error in the mirror specularity and an additional error of 2.8 mrad is introduced by the sun shape. For simplicity, all optical errors can be treated together in an optical error of around 5 mrad (Zhu, 2013; Heimsath et al., 2014). Finally, the exactitude in the calculation of sun position can be evaluated by comparing the results of Spencer's relationship versus the more exact PSA algorithm (Reda and Andreas, 2008), which calculates the solar position with an exactitude of ±0.0003°. This improvement gives small differences (around 2%) in the calculation of the non-illuminated length.

Adimensional parameters were defined, using the height H as the characteristic length. Thus, L_i/H, D_i/H, Z/H, and F_i/H are the adimensional non-illuminated length, horizontal mirror distance, absorber length, and focal mirror distance, respectively. Thus, for a fixed height of the absorber H, different geometries described by D_i/H (or, alternatively, F_i/H) and Z/H can be analyzed.

2.1. Instantaneous $\hat{L}_i$ and end loss factor $f_{end,i}$

The adimensional non-illuminated length $\hat{L}_i = L_i/H$ is a function of the solar angles and the mirror position. This length was obtained from a 3D analysis of the intersection of a plane containing the solar vector and the mirror normal vector, and an infinite line representing the absorber

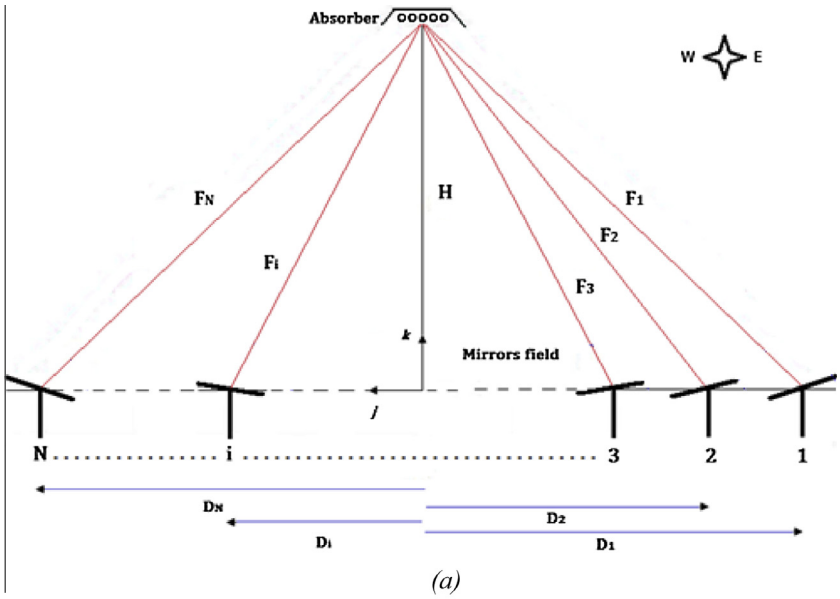

(a)

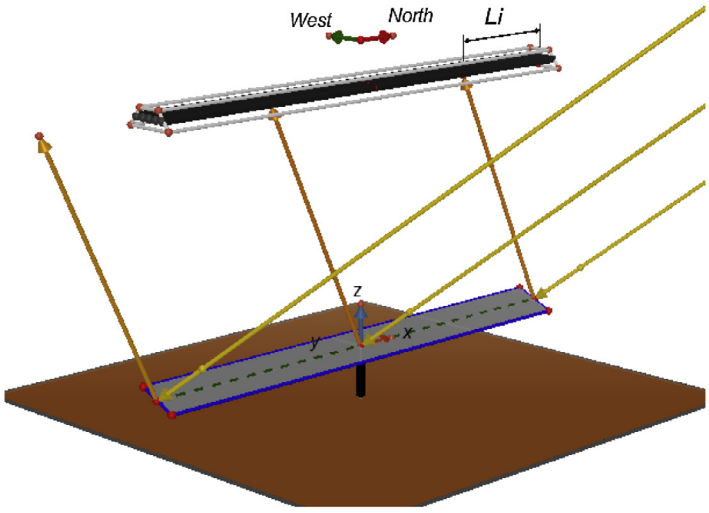

(b)

Fig. 1. (a) Schematic of a North–South LFC with N mirrors. D_i is the horizontal distance between the i mirror centerline and the solar absorber line projected on the aperture plane, H is the height from the aperture plane to the absorber, F_i is the focal distance of the i-mirror. (b) Longitudinal sketch of the LFC where Li can be observed.

(see Appendix A). Thus, $\hat{L}_i$ does not depend on the receiver length and it is calculated as:

$$\hat{L}_i = \frac{L_i}{H} = \frac{-(y_s z_i - y_i z_s)\cos\gamma\left(\frac{D_i}{H}\right) + (x_i z_s - x_s z_i)\sin\gamma\left(\frac{D_i}{H}\right) - (x_s y_i - x_i y_s)}{(y_s z_i - y_i z_s)\sin\gamma + (x_i z_s - x_s z_i)\cos\gamma} \quad (2)$$

In the previous equation, (x_s, y_s, z_s) defines the sun position in the sky and it depends on are the zenith angle θ_z and the azimuth angle γ_s. These angles are determined by using the known set of Spencer's relationships given in Duffie and Beckman (2006). The mirror position (x_i, y_i, z_i), derived in Appendix A, depends on the slope β_i and the azimuth angle γ_i of the i mirror. As shown in Eq. (2), $\hat{L}_i$ can take positive or negative values depending on whether the non-illuminated length is shifted towards North or South, respectively. Furthermore, mirrors at the same distances to the East or West of the receiver have symmetrical behavior in a day. Eq. (2) can be particularized for a North–South tracking mirror by considering $\gamma = 90°$ and $\gamma_i = \pm 90°$.

The end loss factor f_{end} is defined as the illuminated fraction of the receiver length (Heimsath et al., 2014), thus, $0 \leqslant f_{end} \leqslant 1$. For a receiver of length Z, and from Eq. (2), this factor can be written for the i mirror as:

$$f_{end,i} = \begin{cases} 1 - \left(\frac{H}{Z}\right)|\hat{L}_i| & 0 \leq |\hat{L}_i| \leq Z/H \\ 0 & |\hat{L}_i| > Z/H \end{cases} \quad (3)$$

At this point, it is worth noticing two important issues. The first one is that $\hat{L}_i$ can take values higher than Z/H. This situation occurs when the non-illuminated length is longer than the receiver length, so $f_{end,i}$ is strictly zero. This situation was included in the second line of Eq. (3). The second issue to be noted is that $\hat{L}_i$ does not depend on the receiver length Z, whereas the end loss factor $f_{end,i}$ do depend on this value. Both $\hat{L}_i$ and $f_{end,i}$ are helpful parameters in the design of LFC systems. Thus, for a given LFC geometry, $\hat{L}_i$ is useful to determine the quantitative value of the non-illuminated length for any receiver length, while $f_{end,i}$ includes the length of the absorber to account for the fraction of the receiver that is illuminated. In addition, the dependence of f_{end} on the inverse of Z in Eq. (3) shows that shorter receivers suffer higher end losses.

2.2. Average daily and annual $\hat{L}_i$ and average annual $f_{end,i}$

The function $\hat{L}_i$ and $f_{end,i}$ given by Eqs. (2) and (3) can be averaged on daily, monthly or annual periods. As explained, $\hat{L}_i$ can take positive or negative values depending on whether the non-illuminated length is shifted towards North or South, respectively. In both cases what influences the end loss is the magnitude of the non-illuminated length (not the shifting direction), so the magnitude (absolute value) of this quantity must be considered when integrating Eq. (2):

$$\hat{L}_{daily,i} = \frac{1}{(\omega_{max} - \omega_{min})} \int_{\omega_{min}}^{\omega_{max}} |\hat{L}_i| d\omega \tag{4}$$

$$\hat{L}_{annual,i} = \frac{1}{2\delta_{max}(\omega_{max} - \omega_{min})} \int_{-\delta_{max}}^{\delta_{max}} \int_{\omega_{min}}^{\omega_{max}} |\hat{L}_i| d\omega d\delta \tag{5}$$

For average daily and annual end loss factors, the integration of Eq. (3) gives:

$$f_{end,i}^{daily} = \frac{1}{(\omega_{max} - \omega_{min})} \int_{\omega_{min}}^{\omega_{max}} f_{end,i} d\omega \tag{6}$$

$$f_{end,i}^{annual} = \frac{1}{2\delta_{max}(\omega_{max} - \omega_{min})} \int_{-\delta_{max}}^{\delta_{max}} \int_{\omega_{min}}^{\omega_{max}} f_{end,i} d\omega d\delta \tag{7}$$

The previous equations were evaluated through the commercial software package Engineering Equation Solver (EES, 2014). To compute daily averages of functions depending on ω, the method by Xiao (2012) was used. This method proposes to use unweighted integrals for ω going from ($-60° \leqslant \omega \leqslant 60°$), corresponding to a daily operation from 8 h AM to 4 h PM. The author explains that the real situation is more complicated and varies from one setup to another, but that for most real concentrators the result is a reasonably good estimation. Furthermore, from the operative point of view system with fixed on/off periods are simpler to manage and control. To compute annual average functions, the integral depends on the declination δ, which was evaluated for the range $-23.45° \leqslant \delta \leqslant 23.45°$.

Calculations were made for different latitudes and for a range of D_i/H between 0 (mirror axis below the absorber axis) and 2 (distance from mirror axis to absorber axis twice the absorber height). This range covers a wide variety of small LFC systems. South latitudes were analyzed (North latitudes are symmetrical for days with opposite declinations, that is, same magnitude and opposite sign). The results for instantaneous $\hat{L}_i$, $\hat{L}_{daily,i}$, and $\hat{L}_{annual,i}$ are shown in the next section. Finally, general expressions to calculate $\hat{L}_{annual,i}$ and $f_{end,i}^{annual}$ for any latitude, D_i/H and Z/H were found from a second-order fitting.

3. Results and discussion

3.1. Instantaneous $\hat{L}_i$

$\hat{L}_i$ versus D_i/H was calculated from Eq. (2) at different hours from $-60° < \omega < 60°$ (8 h AM–4 h PM) in the winter and summer solstices (June 21st and December 21st), for four latitudes (0°, −10°, −25° and −40°). Fig. 2 shows the results for −10° and −25° of latitude.

As expected, the magnitude (absolute value) of $\hat{L}_i$ increases with mirror distances D_i/H. In winter, this length is always shifted towards South ($\hat{L}_i < 0$) but, in summer, it depends on the latitude and hour (for latitudes between 0° and the tropic, $\hat{L}_i > 0$; for latitudes between the tropic and the pole, $\hat{L}_i > 0$ during the morning and afternoon and $\hat{L}_i < 0$ near the solar noon). Furthermore, the magnitude of the non-illuminated length is larger for higher latitudes and $\hat{L}_i$ reaches the maximum values at solar noon (both in winter and summer). On the contrary, at latitudes near the tropic $\hat{L}_i$ reaches the minimum value in summer (and the maximum in winter), while at the Equator $\hat{L}_i$ remains constant during the whole day (both in the winter and in the summer). In this case, the sun path lies on a plane normal to the system axis, so $\hat{L}_i$ is constant during the day. The non-illuminated length is shifted to North in the summer and to South in the winter.

Comparisons with instantaneous values given in the literature (Shaoxuan and Chaofeng, 2011) for the non-illuminated length of a North–South LFC at a latitude of 25.01°, $H = 10$ m, and for distances D_i/H between 0.25 and 2, the difference was below 0.02 m for the equinocces, that is, a difference below 0.2%.

3.2. Daily adimensional non-illuminated length $\hat{L}_{daily,i}$

Eq. (4) was used to calculate the daily value of the non-illuminated length versus D_i/H for the average days of winter (June 11th), spring (September 15th), summer (December 10th), and autumn (March 16th). The results for -25° and −10° are shown in Fig. 3.

The average daily non-illuminated length increases with D_i/H in all seasons and latitudes. At a given latitude, $\hat{L}_{daily,i}$ is higher in winter. This value is higher at higher latitudes. Additional calculations of the average monthly non-illuminated length were compared with average daily values calculated for the mean days of each month and a maximum difference of 5% was found for the worst

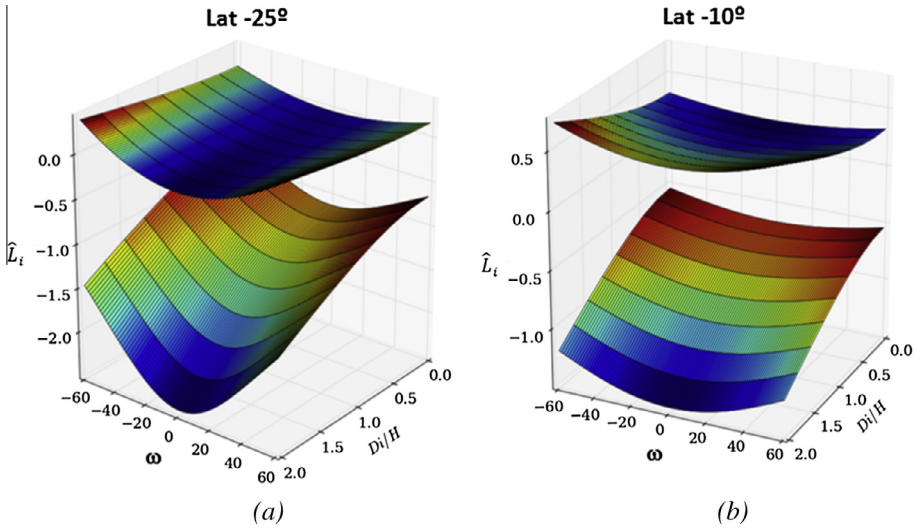

Fig. 2. Instantaneous $\hat{L}_i$ versus D_i/H and solar hour ω for solstices of winter (June 21st, lower surface) and summer (December 21st, upper surface), for latitudes of (a) −25°, and (b) −10°, for a North–South tracking LFC.

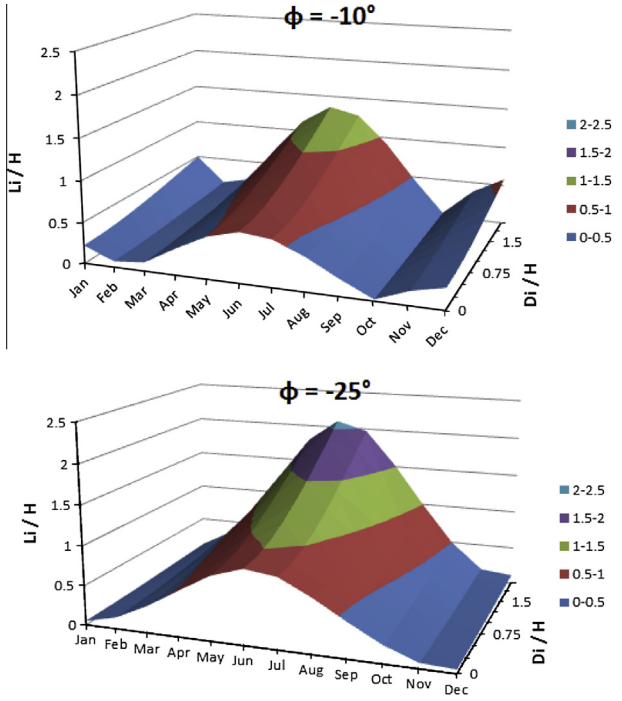

Fig. 3. Average daily $\hat{L}_{daily,i}$ versus D_i/H for the mean days of each month, for different South latitudes (−10° and −25°).

situation (in the winter at high latitudes). Thus, it can be concluded that for medium and low latitudes, the daily value $\hat{L}_{daily,i}$ is a good approximation of the monthly average value.

3.3. Annual adimensional non-illuminated length $\hat{L}_{annual,i}$

For the annual non-illuminated length, instead using D_i/H, the adimensional focal distance F_i/H was used, where:

$$F_i/H = \sqrt{(D_i/H)^2 + 1} \tag{8}$$

Eqs. (5) and (8) was used to calculate the ratio $\frac{\hat{L}_{annual,i}}{F_i/H}$ versus the square of the latitude. The results are shown in Fig. 4.

As expected, at higher latitudes $\frac{\hat{L}_{annual,i}}{F_i/H}$ is also higher. The curve can be reasonably fitted by a first order function of the type:

$$\frac{\hat{L}_{annual,i}}{F_i/H} = A\phi^2 + B \tag{9}$$

where $A = 304.45 \times 10^{-6}$, $B = 212.29 \times 10^{-3}$, and $R^2 = 0.9995$ (Fig. 4).

3.4. Estimation of $f_{end,i}^{annual}$

It is more complicated to achieve a general equation for $f_{end,i}^{annual}$ in a similar way of the previous one because of the dependence of Eq. (7) on the receiver length. But the problem can be faced by realizing that Eq. (9) in fact represents the annual non-illuminated length of a sufficiently long receiver (that is, a receiver with $|\hat{L}_i| < Z/H$ at any time). Then, an expression similar to Eq. (3) can be formulated for the annual average end loss factor:

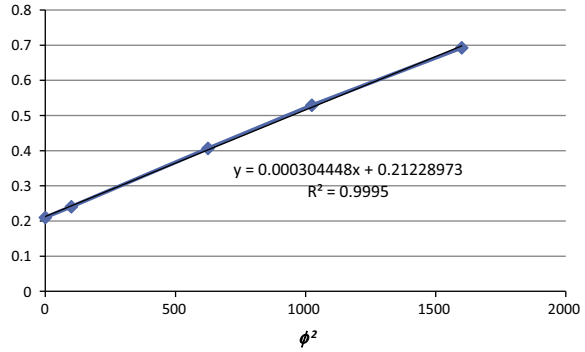

Fig. 4. $\frac{\hat{L}_{annual,i}}{F_i/H}$ as a function of the square of the latitude.

$$f_{end,i}^{annual} = 1 - \left(\frac{H}{Z}\right)\hat{L}_{annual,i}g_{corr} \quad (10)$$

where $\hat{L}_{annual,i}$ is calculated through Eq. (9) and g_{corr} is 1 for receivers that have $|\hat{L}_i| < Z/H$. Thus, for shorter receivers that have $|\hat{L}_i| < Z/H$ a corrective function g_{corr} ($0 \leqslant g_{corr} \leqslant 1$) is applied to $\hat{L}_{annual,i}$ in order to account for the finite receiver length (see Appendix B). In practice, g_{corr} influences more the mirrors placed at higher distances from the receiver, for very short receivers ($Z/H < 1$), and or for sites at high latitudes, as shown in Table B.1.

Eqs. (9) and (10) allow the estimation of the average annual $\hat{L}_{annual,i}$ and the end loss factor for a mirror of a LFC system with any geometric characteristics of D_i, H, and Z and at any latitude between 0° and ±40°. These equations were tested against the exact integral solution and values between 0.2% and 5.0% were found, where the worst situation corresponds to high latitudes ($\phi = -40°$).

Finally, the dependence of the average annual end loss factor on the receiver length is shown in Fig. 5, where the calculations were made for the central mirror ($D_i/H = 0$). As expected, $f_{end,i}^{annual}$ sharply increases for Z/H below 1.5. The average annual end loss factor is higher than 0.9 for $Z/H > 2$ (at low latitudes), $Z/H > 3.75$ (at tropics) and $Z/H > 6$ (at high latitudes). That is, the higher the latitude, the higher the influence of the receiver length on the end losses.

4. Extension to the mirror field and for any orientation

4.1. Effective distance for the mirror field

The annual non-illuminated length $\hat{L}_{annual,i}$ given by Eq. (9) is valid for individual mirror rows. The transition to the whole mirror field can be done by using an effective distance F_{eff}, defined as the distance at which the Eq. (9) equals the mean value of the non illuminated length of the whole field. Thus, if W_{field} the distance from the center of the field to the last mirror, then:

$$\hat{L}_{annual}|_{F_{eff}/H} = \frac{1}{\sqrt{(W_{field}/H)^2 + 1} - 1} \times \int_1^{\sqrt{(W_{field}/H)^2}} \hat{L}_{annual}\left(\frac{F_i}{H}\right) d\left(\frac{F_i}{H}\right) \quad (11)$$

Replacing in Eq. (11) the expression for $\hat{L}_{annual}$ given by Eq. (9) and solving the integral, F_{eff} results:

$$F_{eff} = \frac{1}{2}\left(\sqrt{(W_{field})^2 + H^2} + H\right) \quad (12)$$

From Eq. (8) and Eq. (12), D_{eff} can be obtained. The behaviour of D_{eff} with W_{field} is linear ($R^2 = 0.997$), so the following simplified expression (for $W_{field}/H < 2$) can be used:

$$D_{eff} = 0.653 W_{field} \quad (13)$$

The effective distance given by Eq. (13), or the effective focal distance given by Eq. (12), can be used to predict the behavior of the whole mirror field in Eqs. (9) and (10). Heimsath et al. (2014) suggested an effective distance between the receiver and axis of rotation at a quarter of the aperture plane width, which gives $D_{eff} = 0.5 W_{field}$. This value is lower to the one we have found.

4.2. Generalization to any orientation of the mirror field

The analysis of the previous sections was made for a North–South LFC, but it can be extended to LFCs with different orientations, that is, with different azimuths γ. The method to obtain a generalized expression is similar to that of Section 4. In this case, a set of calculated values of $\hat{L}_{annual,i}$ for different latitudes (0° to −40°, at steps of 5°) and azimuths (90°, 105°, 120°, 135°, 150°, 165° and 180°) was generated for different adimensional focal distances F_i/H. Fig. 6 shows the behavior of $\frac{\hat{L}_{annual,i}}{F_i/H}$ versus the square of the latitude. This behavior is represented by:

$$\frac{\hat{L}_{annual,i}}{F_i/H} = A'(\gamma)\phi^2 + B'(\gamma) \quad (14)$$

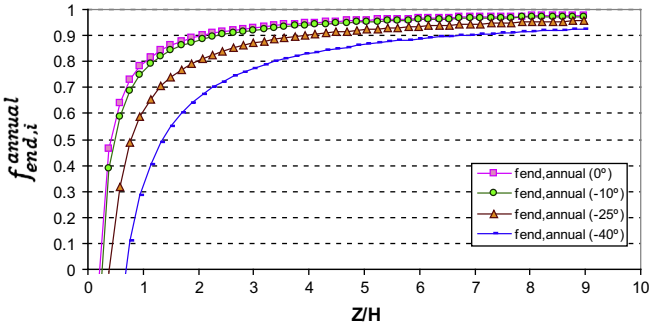

Fig. 5. Average annual end loss factor as a function of the adimensional receiver length Z/H, for the central mirror ($D_i/H = 0$) and at different latitudes.

Table B.1
Correction factor g_{corr} for $\hat{L}_{annual,i}$.

D_i/H	$H/Z = 0.25$	$H/Z = 0.5$	$H/Z = 1$	$H/Z = 1.5$	
0	1	1	0.91	0.75	Lat ±40°
0.5	1	1	0.87	0.70	
1	1	0.98	0.78	0.60	
1.5	1	0.94	0.67	0.49	
2	1	0.87	0.57	0.41	
0	1	1	1	0.92	Lat ±25°
0.5	1	1	0.99	0.88	
1	1	1	0.94	0.77	
1.5	1	1	0.85	0.66	
2	1	0.99	0.75	0.57	
0	1	1	1	1	Lat ±10°
0.5	1	1	1	1	
1	1	1	1	0.96	
1.5	1	1	1	0.88	
2	1	1	0.94	0.80	
0	1	1	1	1	Lat 0°
0.5	1	1	1	1	
1	1	1	1	1	
1.5	1	1	1	0.98	
2	1	1	1	0.91	

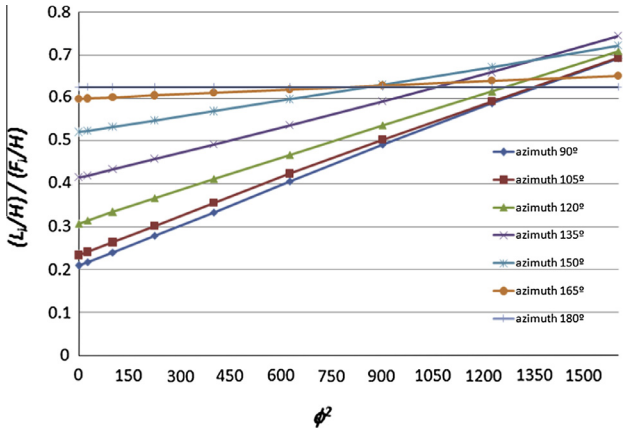

Fig. 6. Average annual $\frac{\hat{L}_{annual,i}}{F_i/H}$ versus the square of the latitude, for different orientations of the LFC system. A linear behavior is observed.

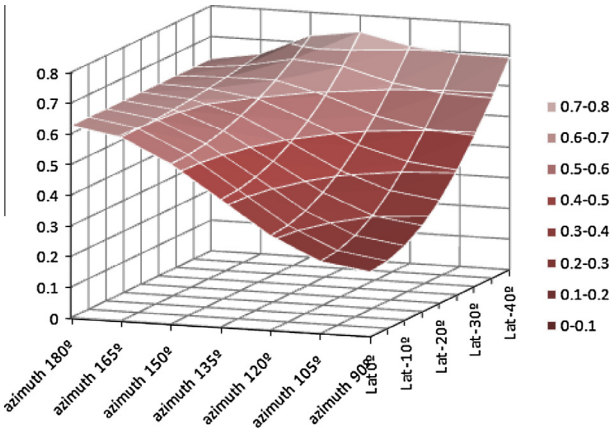

Fig. 7. Average annual $\frac{\hat{L}_{annual,i}}{F_i/H}$ versus latitude and LFC azimuth. As expected, the minimum non-illuminated length is obtained for LFCs oriented in the North–South direction and for latitudes near the Equator.

where $A'(\gamma)$ and $B'(\gamma)$ where obtained for each azimuth γ by the least square fitting method (Table 1). The dependence of A' and B' with the azimuth was described by functions of third order ($R^2 = 0.9943$ and 0.9999, respectively). Thus, the resulting equation is:

$$\hat{L}_{annual,i} = \left(\sqrt{\left(\frac{D_i}{H}\right)^2 + 1}\right)\left[A'(\gamma)\phi^2 + B'(\gamma)\right] \quad (15)$$

where

$$A'(\gamma) = (0.0625\gamma^3 - 27.5625\gamma^2) \times 10^{-8} + (3.5547\gamma - 112.1923) \times 10^{-5}, \text{and}$$

$$B'(\gamma) = (-0.1299\gamma^3 + 52.8844\gamma^2) \times 10^{-5} - 0.0645\gamma + 2.6841$$

In the case of North–South tracking ($\gamma = 90°$), Eq. (15) is equal to Eq. (9).

Fig. 7 shows a 3D plot of $\frac{\hat{L}_{annual,i}}{F_i/H}$ versus latitude and LFC azimuth. As expected, the minimum non-illuminated length is obtained for LFCs oriented in the North–South direction and for latitudes near the Equator. Deviations of 10° from the North–South direction result in errors of around 3.4% in the worst case.

5. Experimental setup

5.1. Experimental setup and methodology

The measurement of the non illuminated length on the receiver of an LFC system is not simple and, to the best of our knowledge, there is little experimental information found in the literature, which was obtained through solar sensors or thermography. In this paper, the non-illuminated length was measured through digital imaging analysis. As shown in the following sections, the proposed experimental method allowed us to determine the instantaneous non-illuminated length with an average error of around 7%.

The prototype is a North–South LFC installed at the INENCO experimental campus in Salta, Argentina (24.7° South latitude, 65.4° West longitude). The geometry of the LFC is shown in Table 2. The 9 mirrors in the field were numbered from 1 (at the East end, $D_1 = -4.92$ m) to 9 (at the West end, $D_9 = 4.92$ m); thus, the mirror number 5 ($D_5 = 0$ m) was placed right below the receiver. The glass cover in the bottom of the receiver was removed in order to obtain clearer images of the shading profile. Firstly, a selected mirror was independently positioned in order to reflect the incident radiation onto the receiver. Then, a photograph was taken with a digital camera installed exactly below the receiver. Special care was taken with the digital camera, for which automatic focus and brightness were set off in order to avoid automatic modifications of the image. This process was repeated for each mirror in the LFC field. Photographs were taken in clear days in the

Table 1
Fitting values of A' and B' for different azimuths.

Azimuth γ	A'	B'	R^2
90	5.07414E−05	0.03538162	0.9995
105	4.82294E−05	0.03960214	0.9993
120	4.17403E−05	0.05166042	0.9999
135	3.40269E−05	0.06879188	0.9991
150	2.08816E−05	0.08669693	0.9997
165	3.40865E−05	0.59889313	0.9989
180	0	0.62592372	1

Table 2
Geometrical and constructive specifications of the tested LFC prototype.

Item	Value
Collection area	43.2 m^2
Number of mirrors, N	9
Mirror width	0.80 m
Spacing between mirror centers	1.23 m
Position of mirror surface from ground	1.00 m
Absorber length, Z	6.00 m
Position of absorber tubes from reflectors level, H	5.36 m
Number of tubes of the receiver	5
Receiver width	0.22 m
Kind of cavity receiver	Trapezoidal

period that goes from December/2013 to May/2014, at time steps of around 20–30 min.

A post-processing image analysis was performed in order to eliminate the errors due to the slope of the absorber and/or the inexact alignment of the camera with respect to the receiver. Thus, each photograph was processed with SCIPRO, a software for image processing developed at INENCO (Hoyos and De Paul, 2013). This software makes the calculations needed to transform the data in projective geometry to the Euclidean plane geometry. This transformation requires the specification of four reference points, which in this case were selected on the tube planes, and a coordinate center as shown in Fig. 8d. Once the image was corrected, the non-illuminated length at the central receiver axis was determined by pixel count on the image. Finally, this length was divided by H to obtain the adimensional value $\hat{L}_i$.

5.2. Results

Fig. 8 shows the measurements performed on the first and seventh mirrors ($D_1/H = -0.92$, $D_7/H = 0.46$) on March 21st (equinox) and on April 16th, 2014.The adimensional length $\hat{L}_i$ and the non-illuminated length L_i (m) are shown in the primary and secondary vertical axes, respectively. As expected from the analysis of Section 3.1, the maximum non illuminated length is reached at solar noon and it is around 5 m (first mirror) and 4.1 m (seventh mirror) on April 16th. Then, at this hour $f_{end,1} = 0.17$ and $f_{end,7} = 0.32$, that is, only 17% of the receiver is illuminated by the first mirror and 32% by the seventh mirror. The average daily values of the end loss factor for March 21st were 0.6 (first mirror) and 0.68 (seventh mirror) while on April 16th these values were 0.3 (first mirror) and 0.45 (seventh mirror).

The theoretical values obtained from Eq. (1) are also shown in Fig. 8. A good agreement between the theoretical and experimental values was found with RMSE values of 6.9% and 5.2% (first mirror), and 4.1–2.5% (seventh mirror), on March 21st and April 16th, respectively. The maximum differences between the theoretical and experimental values occurred when the sun altitude was low (in the morning and in the afternoon). These differences were higher for the first mirror (around 0.35 m) than for the seventh mirror (around 0.14 m). These values correspond to relative errors of around 10% and 5% for the first and seventh mirror, respectively. A possible explanation of this difference is that the seventh mirror is at a shorter distance from the central axis and, thus, it was less influenced by optical errors. Some errors are intrinsic to the mirrors

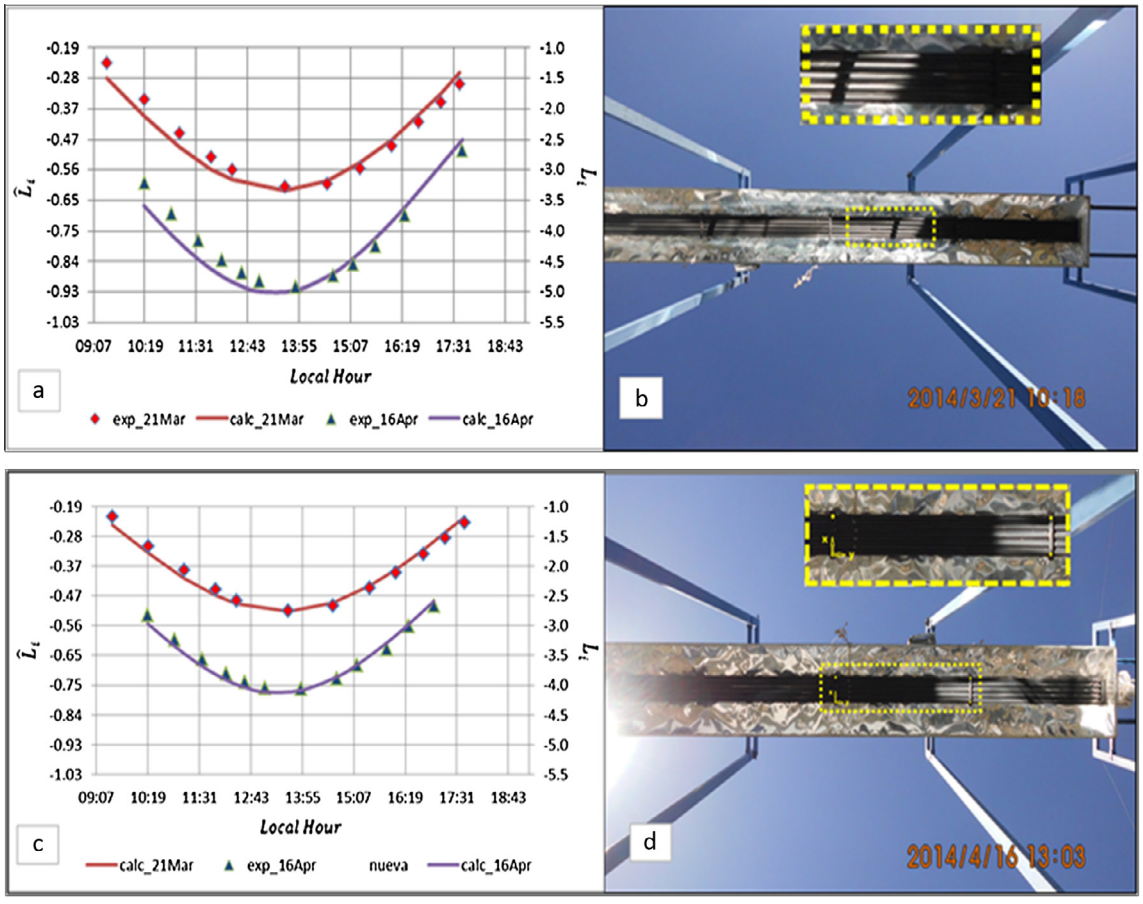

Fig. 8. Experimental and theoretical instantaneous $\hat{L}_i$ for the first mirror situated at $D_1/H = -0.92$ (a–b) and for the seventh mirror at $D_7/H = 0.46$ (c–d). The measurements were taken on March 21st and April 16th, 2014.

(slope, astigmatism of the mirror surface, non horizontality of the receiver or mirror axes) and others are the result of the measurement method (uncertainties in the determination of the central point in the illumination profile, errors in the location of the points of reference, errors of the camera optics/software, etc.). Such errors are more influential for higher focal distances, in particular the astigmatism of the mirrors (Mertins, 2009). In this case, the slightly parabolic profile of the mirrors produces the reflected rays not to converge at a clear focal line but at a zone delimited by the catacaustic of the parabola. This zone of convergence changes of shape and position during the day. The quantitative analysis of the optical errors and the whole optical performance of the LFC is out of the scope of this paper. Finally, it is worth noting that the measurements were carried out in autumn; consequently, greater errors could be expected for measurements in other seasons, especially in winter.

5.3. Estimation of the average daily and annual end loss factor

The average daily end losses of the INENCO prototype were calculated using Eqs. (3) and (6). The results are shown in Fig. 9 for the average day of each month along the year. The geometric variables for this prototype are (Table 2): $Z/H = 1.12$, $|D_i/H| \leqslant 0.92$. As shown, the theoretical values in March and April for the first and seventh mirrors agree with the values obtained from the experimental measurements. The results also show that end losses in June are so high that the absorber receives only around 18% of the energy collected by the central mirror. On the contrary, in December the end loss factor is between 0.92 and 0.95 for all mirrors, that is, a high portion of the reflected energy is intercepted by the absorber.

The estimation of the annual end loss factor can be found from Eq. (10) with the corrections given in Appendix B. Table 3 shows the results for each mirror. Average annual end loss factors vary from 0.57 to 0.65 and, as expected, mirrors at longer distances have lower end loss factors. The short length of the receiver causes the loss of around 39% (in average) of the solar radiation collected by the mirror field. This is a very noticeably percentage and some actions should be taken to overcome this problem. Some authors have proposed different solutions: to enlarge the receiver length, to incline the mirrors at a position different from horizontal plane, to add an auxiliary reflective surface at the ends of the receiver, or to enlarge the mirror field. In the studied small LFC – designed for steam applications – the adopted solution was to mount the receiver on rails, in order to displace it towards the South when necessary (for example, in winter the receiver is displaced around 4 m).

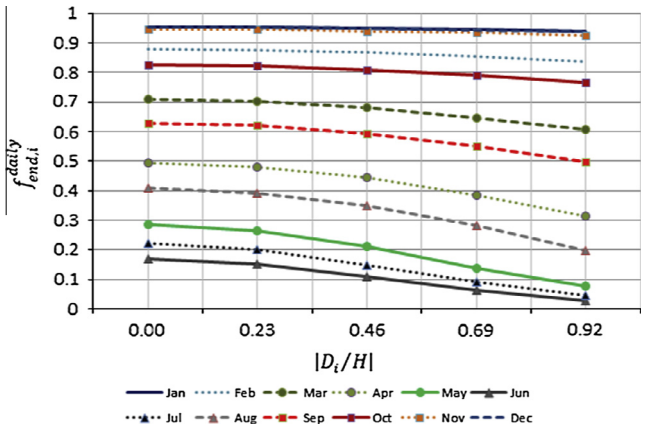

Fig. 9. $f_{end,i}^{daily}$ versus $|D_i/H|$ for monthly average days in Salta (latitude: −24.7°).

Table 3
Estimation of the annual end loss and average non-illuminated length for each mirror for the LFC at INENCO campus.

Number of mirror (i)	D_i/H	f_{annual}
1	−0.92	0.57
2	−0.69	0.59
3	−0.46	0.61
4	−0.23	0.63
5	0	0.65
6	0.23	0.63
7	0.46	0.61
8	0.69	0.59
9	0.92	0.57

6. Conclusions

Optical end losses of LFC concentrators are caused by both, the geometry of the mirror field and the site latitude. These losses are important in a short LFC as they limit the energy reflected by the mirror field that is received by the absorber. End losses have stronger influence on sites at high latitudes and it could cause the absorber to be completely in shadow in winter days. Thus, in rectangular configurations, in which the receiver length equals the mirror length, the receiver length must exceed the critical minimum value that ensures that a reasonable amount of solar radiation will reach the absorber each day throughout the year.

The contribution of this paper is a general expression to estimate the average annual end loss factor of a rectangular LFC, which is simpler to use than conventional ray-tracing techniques. This equation is valid at any latitude between 0° and ±40° and azimuth of the LFC system, with an error of 0.2–5.0% between this equation and the exact integral solution. The model showed good agreement between theoretical and experimental values found by measuring $\hat{L}_i$ on a North–South LFC installed at the INENCO experimental campus. The results confirm that end loss is underestimated by calculation for the central mirror only. We are currently in the process of investigating the optimal mirror spacing in order to optimize the land use and the efficiency of LFC systems. Mirror curvature will be included in a future improved model.

In non-rectangular LFC, end losses can be reduced by increasing the length of the mirror field while keeping fixed the absorber length, which leads to a non-rectangular geometry. In the future, the results obtained in this paper will be extended to cover this configuration. In this case, the optimal length of the mirror field depends on an economic cost-benefit balance, and further work is needed to assess the value that minimizes the costs and maximizes the energy collection of short LFC receivers.

Acknowledgements

This work was supported by projects of Ministerio de Ciencia, Tecnología e Innovación Productiva de la Nación (PFIP 2008), CONICET and Universidad Nacional de Salta.

We are particularly grateful to Dr. Luis Saravia, who conducts the projects. We also thank Prof. Daniel Hoyos for his valuable suggestions and discussions on the experimental methodology and Prof. Soledad Loutayf for her assistance in language and paper writing.

Appendix A.

Derivation of the adimensional non-illuminated length $\hat{L}_i$

The sun position in polar coordinates is determined by the solar zenith and azimuth angles (θ_z, γ_s), and they are calculated by the Spencer's relationship given in Duffie and Beckman (2006), which depends on the latitude ϕ, declination δ, and solar hour ω:

$$\cos\theta_z = \cos\phi\cos\delta\cos\omega + \sin\phi\sin\delta \tag{A.1}$$

$$\gamma_s = sign(\omega)\left|\cos^{-1}\left(\frac{\cos\theta_z\sin\phi - \sin\delta}{\sin\theta_z\cos\phi}\right)\right| \tag{A.2}$$

$$\delta = 23.45\sin\left(360\frac{284+n}{365}\right) \tag{A.3}$$

The sun's position, relative to the axis of rotation of the LFR elements, is determined from the solar profile angle. The profile angle α_p, can be found by (Duffie and Beckman, 2006),

$$\tan\alpha_p = \frac{\tan(90-\theta_z)}{\cos(\gamma_s-\gamma)} \tag{A.4}$$

where the profile angle α_p and the azimuth angle γ vary between 0° and 180°.

As the sun moves in the sky, each mirror must be positioned at an angle β_i' in order to reflect the solar radiation to the absorber. β_i' is positive when the mirror surface faces west. This angle changes with time, latitude and the mirror position. If the mirror is considered as an ideal reflecting surface, then β_i' is defined as:

$$\beta_i' = \left[\frac{\alpha_p + \operatorname{atan}\left(\frac{H}{D_i}\right)}{2}\right] - 90^\circ \tag{A.5}$$

In spherical coordinates, the mirror position can be defined by the surface azimuth angle γ_i and the slope β_i of the mirror surface:

$$\gamma_i = sign(\beta_i')*90^\circ \tag{A.6}$$

$$\beta_i = |\beta_i'| \tag{A.7}$$

In the following, the reflection of the sunray by the mirror is supposed to occur in a point of the mirror centerline. Fig. A.1 shows the three points involved in the calculation: the origin (0, 0, 0) which is placed at the center of the mirror, the normal to the mirror surface $P_i = (x_i, y_i, z_i)$, and the sun direction which is described by the zenith and azimuth angles (θ_z, γ_s), or in Cartesian coordinates by the unit vector $P_s = (x_s, y_s, z_s)$. For a tracking mirror with any orientation γ_i, P_i and P_s are calculated as:

$$x_s = -\sin\theta_z\cos\gamma_s \tag{A.8}$$

$$y_s = \sin\theta_z\sin\gamma_s \tag{A.9}$$

$$z_s = \cos\theta_z \tag{A.10}$$

$$x_i = -\sin\beta_i\cos\gamma_i \tag{A.11}$$

$$y_i = \sin\beta_i\sin\gamma_i \tag{A.12}$$

$$z_i = \cos\beta_i \tag{A.13}$$

The specular reflection law establishes that the incident and reflected rays lie in the same plane, defined by the algebra as the plane containing the points P_s, P_i and (0, 0, 0):

$$\begin{vmatrix} x & y & z \\ x_s & y_s & z_s \\ x_i & y_i & z_i \end{vmatrix} = 0 \tag{A.14}$$

The result for this determinant gives the equation of the plane containing the incident and the reflected rays:

$$(y_sz_i - y_iz_s)x + (x_iz_s - x_sz_i)y + (x_sy_i - x_iy_s)z = 0 \tag{A.15}$$

The absorber can be represented by an infinite straight line in $\mathbb{R}^3$, whose parametric equation is:

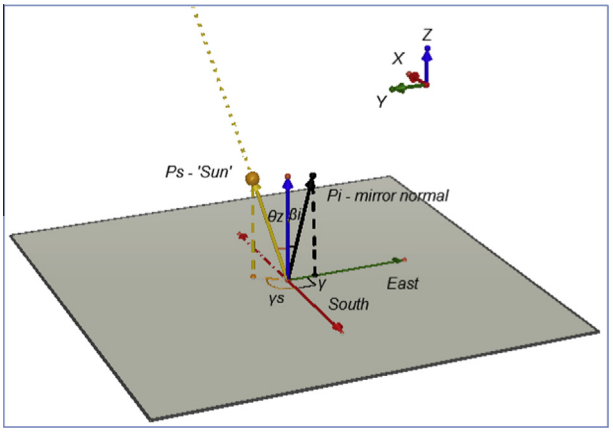

Fig. A.1. Sun ray direction (P_s) and normal to the mirror surface (P_i) for a North–South tracking mirror ($\gamma_i = \pm 90°$). The origin (0, 0, 0) is placed at the mirror center.

$$\begin{cases} X_{abs} = X_0 + \lambda u_x \\ Y_{abs} = Y_0 + \lambda u_y \\ Z_{abs} = Z_0 + \lambda u_z \end{cases} \quad (A.16)$$

where (X_0, Y_0, Z_0) is the central point of absorber and (u_x, u_y, u_z) is a unit vector in the direction of the absorber. Thus, if the absorber is at a distance D_i to the East of the mirror i, at a height H above the mirror plane, and at an azimuth γ, then:

$$\begin{cases} X_0 = D_i \cos\gamma \\ Y_0 = -D_i \sin\gamma \\ Z_0 = H \end{cases} \quad (A.17)$$

$$\begin{cases} u_x = \sin\gamma \\ u_y = \cos\gamma \\ u_z = 0 \end{cases} \quad (A.18)$$

λ is obtained by replacing (A.16) in (A.15):

$$\lambda = \frac{-(y_s z_i - y_i z_s)u_y D_i + (x_i z_s - x_s z_i)u_x D_i - (x_s y_i - x_i y_s)H}{(y_s z_i - y_i z_s)u_x + (x_i z_s - x_s z_i)u_y + (x_s y_i - x_i y_s)u_z} \quad (A.19)$$

λ is the non-illuminated length L_i, so the dimensionless non illuminated length of the absorber is given by:

$$\hat{L}_i = \frac{L_i}{H} = \frac{-(y_s z_i - y_i z_s)\cos\gamma\left(\frac{D_i}{H}\right) + (x_i z_s - x_s z_i)\sin\gamma\left(\frac{D_i}{H}\right) - (x_s y_i - x_i y_s)}{(y_s z_i - y_i z_s)\sin\gamma + (x_i z_s - x_s z_i)\cos\gamma} \quad (A.20)$$

The value of L_i is positive or negative depending on the direction of the reflected ray. Thus, $L_i > 0$ if the reflected beam is shifted towards North and $L_i < 0$ if it is shifted towards South. This is valid for any LFC axis orientation except for East–West orientation. For this specific case ($\gamma = 180°$), $L_i > 0$ if the reflected beam is shifted towards West of absorber and $L_i < 0$ otherwise.

Fig. A.2 shows a scheme of the non-illuminated length for September 15th (11:25 AM), for South latitude $\phi = -24.7°$. The mirror is placed at $D_i = -3.69$ m, the absorber height is $H = 5.36$ m. The declination and sun position are calculated using Eqs. (A.1)–(A.3). Thus, through Eqs. (A.8)–(A.13), the vectors P_s, P_i are calculated. Finally, the non-illuminated length is calculated through Eq. (A.20) giving −3.40 m (the negative sign indicates that the non-illuminated length is shifted towards South).

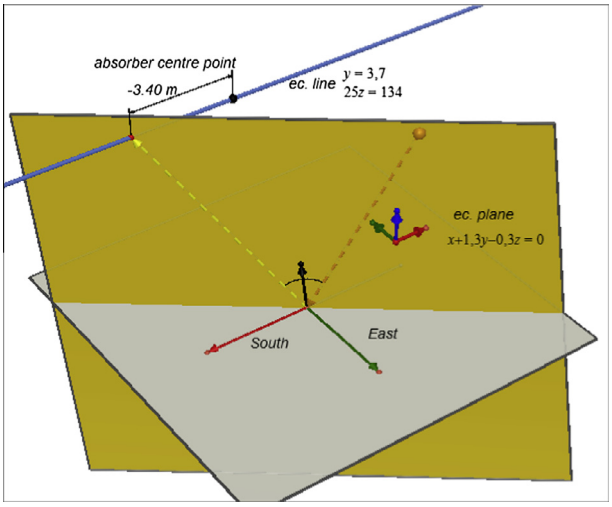

Fig. A.2. Scheme of the non-illuminated length for September 15th (11:25 AM), for latitude −24.7°. The mirror is placed at $D_i = -3.69$ m, the absorber height is 5.36 m, and the resulting non-illuminated length is −3.40 m (the negative sign indicates that the non-illuminated length is shifted towards South).

Appendix B.

Correction factor g_{corr} for North–South tracking axis

A correction factor is included into Eq. (10) in order to account for the receiver length:

$$g_{corr} = \frac{1 - f_{end,i}^{annual}}{(H/Z)\hat{L}_{annual,i}} \quad (B.1)$$

where $f_{end,i}^{annual}$ and $\hat{L}_{annual,i}$ are calculated from Eqs. (5) and (7). Thus,

$$f_{end,i}^{annual} = 1 - \frac{H}{Z}\hat{L}_{annual,i} g_{corr} \quad (B.2)$$

Table B.1 gives the values of the correction factor for different latitudes, receiver lengths H/Z and distances D_i/H, calculated through Eq. (B.1) by using EES numerical software. Values of g_{corr} not included in the table can be obtained by linear interpolation.

References

Bermejo, P., Pino, F.J., Rosa, F., 2010. Solar absorption cooling plant in Seville. Sol. Energy 84 (8), 1503–1512.

Buie, D., Dey, C.J., Mills, D., 2002. Optical considerations in line focus fresnel concentrators. In: 11th International Solar Paces Conference, September 2002, Zürich, Switzerland, pp. 197–203.

Duffie, J.A., Beckman, W.A., 2006. Solar Engineering of Thermal Processes, third ed. John Wiley & Sons, New York, p. 14.

EES, 2014. <http://www.fchart.com/ees/>.

Häberle, A., Berger, M., Luginsland, F., Zahler, C., Baitsch, M., Henning, H., Rommel, M., 2006. Linear concentrating fresnel collector for process heat applications. Solar Paces. In: 13th International Symposium on Concentrating Solar Power and Chemical Energy Technologies, June 20–23, Sevilla, España, 2006.

Heimsath, A., Bern, G., van Rooyen, D., Nitz, P., 2014. Quantifying optical loss factors of small linear concentrating collectors for process heat application. Energy Proc. 48, 77–86.

Hoyos, D., De Paul, I., 2013. Sistema de estereografía digital de bajo costo. In: XXXVI Reunión de Trabajo de la Asociación Argentina de Energías Renovables y Medio Ambiente, pp. 08.163-08.170, Argentina. Available at: <http://asades.inenco.net/index.php/asades/asades2013/paper/viewFile/1162/219> (last accessed: 26.05.14).

Huang, W., Han, Z., 2012. Theoretical analysis of error transfer from the surface slope to the reflected ray and their application in the solar concentrated collector. Sol. Energy 86, 2592–2599.

Mertins, M., 2009. Technische und wirtschaftliche Analyse von horizontalen Fresnel-Kollektoren. Ph.D. thesis, Universität Karlsruhe.

Rawlins, J., Ashcroft, M., 2013. Report: small scale concentrated solar power – a review of current activity and potential to accelerate employment, carbon trust. Available at: <https://www.gov.uk/government/uploads/system/uploads/attachment_data/file/191058/small_scale_concentrated_solar_power_carbon_trust.pdf>.

Reda, I., Andreas, A., 2008. Solar Position Algorithm for Solar Radiation Applications. NREL/TP-560-34302. Available at: <http://www.nrel.gov/docs/fy08osti/34302.pdf> (last accessed: 28.07.14).

Shaoxuan, Pu, Chaofeng, Xia, 2011. End-effect of linear Fresnel collectors. Power and Energy Engineering Conference (APPEEC), March 2011, Asia–Pacific, pp. 25–28.

Sultana, T., Morrison, G.L., Rosengarten, G., 2012. Thermal performance of a novel rooftop solar micro-concentrating collector. Sol. Energy 86 (7), 1992–2000.

Ulmer, S., Heinz, B., Pottler, K., Lupfert, E., 2009. Slope error measurements of parabolic troughs using the reflected image of the absorber tube. J. Sol. Energy Eng.-Trans. ASME 131 (1).

Xiao, Gang, 2012. Tilting mirror strips in a linear Fresnel collector. University of Nice, France. Available at: <http://hal.archives-ouvertes.fr/docs/00/67/52/22/PDF/tilt.pdf>, p. 4.

Zhu, G., 2013. Development of an analytical optical method for linear Fresnel collectors. Sol. Energy 94, 240–252.